Dalton Transactions

ROYAL SOCIETY OF CHEMISTRY

PAPER

View Article Online
View Journal | View Issue

Cite this: *Dalton Trans.*, 2026, **55**, 1753

Self-assembled nanocomposite of HKUST-1 and LAPONITE®: towards a hydrogel with high mechanical strength for selective dye adsorption and column chromatographic separation

Jyoti,[a] Chhaya,[a] Vinod Kumar[a] and Anindita Chakraborty *[b]

Received 21st August 2025,
Accepted 11th December 2025

DOI: 10.1039/d5dt02005k

rsc.li/dalton

Herein, we report the synthesis of a novel hydrogel nanocomposite, **HKUST-1@LP**, through the self-assembly of a prototype metal–organic framework (MOF), **HKUST-1** and the nanoclay, LAPONITE® (LP). The nanocomposite was characterized by using different techniques including PXRD, FESEM, EDX, FTIR, TGA, rheology, zeta potential analysis and N_2 adsorption measurements. The resulting composite exhibits significantly enhanced dye adsorption/separation properties compared to its individual parent components and has been exploited as a dye adsorbent and stationary phase for gel-column chromatography. It demonstrates superior capabilities in selective dye adsorption, particularly for cationic dyes such as methylene blue (MB), 229 mg g^{-1}, and rhodamine B (RhB), 212 mg g^{-1}, with adsorption kinetics influenced by temperature. Furthermore, the **HKUST-1@LP** hydrogel separates mixtures of dyes effectively, as was evident from the conducted gel-column chromatography experiments. The **HKUST-1@LP** hydrogel showcases remarkable mechanical robustness and rheological studies revealed higher storage modulus (G') and loss modulus (G'') values for the composite compared to pristine LP, withstanding greater strain levels before structural failure (82.7% for **HKUST-1@LP** hydrogel *vs.* 52.7% for LP). These enhanced mechanical and functional attributes underscore the composite's potential for practical applications in selective dye adsorption and chromatographic separation processes.

Introduction

Metal–organic frameworks (MOFs) have attracted significant attention over the past two decades due to their highly crystalline nature, exceptionally large surface area, structural tunability and their potential in various applications, including catalysis, sensing, drug delivery, adsorption, and separation.[1–11] However, the powdered forms of most MOFs, and thus their poor processability and stability in water,[12,13] limit practical applications as membranes, filters or columns.[14–17] To overcome these issues, MOF composites[18–29] have emerged as new functional materials that offer superior properties, including better solution processability and applications compared to those of the parent materials. In particular, MOF-based hydrogel composites offer significant advantages over powdered materials, as the gels exhibit excellent solution processability and hold great potential for applications in adsorption/separation, optoelectronics, gas storage, catalysis, sensing, and drug delivery.[30–35] However, synthesis of soft gels from rigid MOFs remains a formidable challenge, and requires complex synthetic routes and precise control over the conditions used.[36–42]

Dye adsorption and separation using MOFs is a highly effective method for wastewater treatment and environmental protection by minimizing chemical waste and enabling dye recovery for industrial reuse.[43] When MOFs are packed into chromatographic columns for separation applications, issues such as inhomogeneous packing, the formation of cracks, and high backpressure significantly compromise performance and reproducibility.[14–17] We envisage that a MOF-based hydrogel composite could have enhanced potential for dye capture and separation, owing to the gel network structure in the composite and synergistic effects of the functional parent materials. Furthermore, the gel network structure could potentially prevent the formation of cracks, inhomogeneous distribution of the sample and dead zones when packed into columns for chromatographic separation. To furnish such a composite, we have selected a synthetic nanoclay, LAPONITE® (LP). LP is a synthetic nanoclay having molecular formula $Na^{+}_{0.7}[(Si_8Mg_{5.5}Li_{0.3})O_{20}(OH)_4]^{-0.7}$ with a 2 : 1 layered structure and disk-like particles ~25 nm in diameter and ~1 nm thick, where Li^+ ions partially replace Mg^{2+} ions in the octahedral

[a]*Department of Chemistry, School of Basic Sciences, Central University of Haryana, Mahendergarh 123031, Haryana, India*
[b]*Special Centre for Nano Sciences, Jawaharlal Nehru University, New Mehrauli Road, New Delhi, Delhi 110067, India. E-mail: anindita.chemistry1@gmail.com*

layer, creating a net negative charge balanced by Na^+ ions. In water, Na^+ dissociates, making the sheet faces negatively charged, while the edges, rich in Mg–OH groups, become positively charged at neutral pH, leading to an anisotropic charge distribution.[44] LP is widely recognized for its high dispersibility in water, excellent rheological properties[45–50] and potential use in biomedicine.[51] The fabrication of structurally resilient modulable hydrogels[45] for targeted drug delivery[48] and size-selective catalysis[52] can also be achieved through the strategic synthesis of LP composites. The chemistry of MOF–LP composites is relatively new and their composite gels can be synthesized using a one-pot facile self-assembly process,[33,52] contrary to the traditional but tedious synthetic approaches for gel formation.[14,42] Inspired by the potential of MOF–LP composites and further exploring the potential of LP in MOF chemistry, we present herein the synthesis of a hydrogel nanocomposite termed **HKUST-1@LP**, incorporating the MOF, **HKUST-1**. **HKUST-1** is a prototype MOF known for its large surface area and enhanced thermal stability, making it highly suitable for various applications in adsorption and separation studies.[53–56] We hypothesize that the formation of the **HKUST-1@LP** nanocomposite is facilitated by the charge-assisted self-assembly (Scheme 1) between the two parent materials: **HKUST-1** nanoparticles having negatively charged surfaces (due to the deprotonation of the carboxylic acid linkers)[57] and the LP particles having positively charged edge sites.[44] The resulting composite exhibits superior capabilities in selective dye adsorption, particularly for cationic dyes such as methylene blue (MB) and rhodamine B (RhB). The composite hydrogel was eventually exploited in this study as a stationary phase in chromatographic dye separation from mixtures of cationic and anionic dyes, such as MB and methyl orange (MO).

To the best of our knowledge, such a MOF–clay hydrogel composite serving as a stationary phase in chromatographic dye separation is reported for the first time.

Results and discussion

Synthesis and phase purity

HKUST-1 was synthesized by following a previously reported synthetic procedure.[58] The PXRD pattern of as-synthesized **HKUST-1** matches well with the literature-reported[58] PXRD pattern (Fig. S1). To synthesize the hydrogel nanocomposite, we initially focused on optimizing the reaction conditions for the composite formation. We prepared several batches under varied reaction conditions to identify the optimal parameters (Table S1 and Fig. S2) and selected entry no. 2 (see Table S1), which yielded instant gel formation. The resulting composite was termed **HKUST-1@LP**, which was subsequently used in our work. Briefly, an *ex situ* synthetic approach was used where LP was first dispersed in water, followed by the addition of **HKUST-1** suspension during sonication (see the Experimental section for details). We believe that the composite gel formation is driven by the electrostatic interactions between the negatively charged surface of **HKUST-1** particles (resulting from the deprotonation of –OH groups in the carboxylic acid moieties, forming $–COO^-$ groups)[57] and the positive surface charge at the edges of LP particles (arising from the presence of Mg–OH in LP).[44] The formation of the **HKUST-1@LP** xerogel was verified by its PXRD pattern that revealed the composite is more aligned with pure LP[59] (Fig. S3a), which may be attributed to the higher amount of LP present in the composite. However, to understand the chemical integrity in the **HKUST-1** phase of the composite, we carried out additional experiments. Specifically, **HKUST-1** was immersed in water under identical synthetic conditions to those used for the composite (see the Experimental section for details), and the resulting materials were analyzed by PXRD. The obtained pattern (Fig. S3b) clearly shows that the characteristic diffraction peaks of **HKUST-1** are retained, confirming that the **HKUST-1** framework does not undergo decomposition under the applied conditions (identical to those of the composite synthesis).

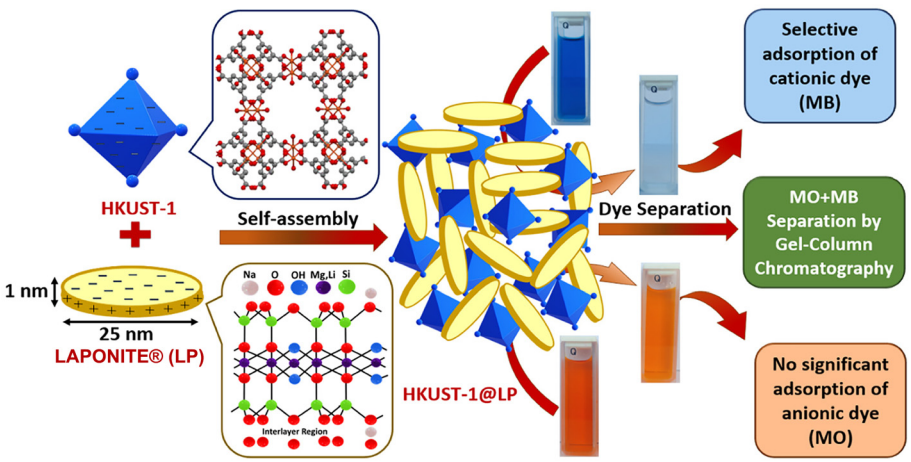

Scheme 1 Schematic representation of the synthesis of **HKUST-1@LP** hydrogel nanocomposite *via* self-assembly of **HKUST-1** with LP. The nanocomposite was used in selective dye adsorption and separation.

IR spectra and thermal stabilities

The FTIR spectrum (Fig. 1) of as-synthesized **HKUST-1** shows the characteristic peaks of **HKUST-1**, as reported in the literature.[60,61] The IR spectrum of LP demonstrates its characteristic structure of clay (Si–O–Si 971 cm^{-1}, Mg–O 649 cm^{-1}) with the presence of a broad O–H stretching frequency band (~3000–3400 cm^{-1}).[59] The FTIR spectral analysis of the **HKUST-1@LP** xerogel confirms the formation of a nanocomposite showing characteristic peaks of **HKUST-1** and LP, such as 1646 cm^{-1}, 1554 cm^{-1}, 1372 cm^{-1} and 729 cm^{-1}, attributed to the ν_{asym}(C═O), C═C, and ν_{sym}(C–O) and Cu–O functionalities derived from the MOF, and the functionality originating from the LP phase with a slight shift in stretching frequencies of Si–O–Si and Mg–O at 968 cm^{-1} and 646 cm^{-1}, respectively, which can be attributed to the interaction of the MOF with LP. The presence of the characteristic peaks attributed to the functional groups arising from the **HKUST-1** further supports the **HKUST-1** phase being retained in the composite without any decomposition.

To ascertain the thermal stability of all the samples, thermogravimetric analysis (TGA) of LP, as-synthesized **HKUST-1** and **HKUST-1@LP** xerogel was carried out (Fig. S4). The TGA results of LP are well-matched with the literature reported values and indicate an initial weight loss of ~13% up to 100 °C attributed to the removal of adsorbed water molecules and negligible weight loss (~5–6%) between 700 and 800 °C because of the presence of phyllosilicates having high heat of resistance.[62,63] TGA of as-synthesized **HKUST-1** reveals an initial weight loss of ~18% at 120 °C, attributed to the water molecules present in the MOF, matching well with results in the literature.[58] The composite xerogel exhibits thermal stability up to 300 °C, which is similar to that of the as-synthesized **HKUST-1**. Beyond this temperature, decomposition of the MOF framework begins. The thermal profile of **HKUST-1@LP** xerogel at temperatures above 300 °C is similar to that of LP, which is maintained up to 700 °C. The plot also indicates that the use of LP does not impact the thermal stability of the **HKUST-1** framework in the hydrogel nanocomposite.

Textural properties

To analyze the textural properties of the samples, we recorded the FESEM data of **HKUST-1** (Fig. S5a) and **HKUST-1@LP** xerogel (Fig. S5b). The particle size of the as-synthesized **HKUST-1** lies in the range of 55–300 nm, within which most particle sizes are in the range of 75–85 nm (Fig. S6). The textural properties of **HKUST-1** are in good accordance with the literature.[58] **HKUST-1@LP** xerogel displays a morphology resembling that of LP[59] (Fig. S5b), which is attributed to the fact that in the composite, **HKUST-1** particles are embedded within the LP layers, which constitutes the higher weight percentage of the composite. Elemental mapping of the **HKUST-1@LP** xerogel reveals that the elements from both the parent materials are uniformly present in the composite, *i.e.*, Cu from the **HKUST-1** MOF and Mg and Na from the LP. The uniform distribution of these elements suggests that the MOF nanoparticles are uniformly distributed throughout the LP matrix, resulting in a homogeneous composite (Fig. S7).

Gas adsorption study

To examine the porous nature and surface area of the samples, N_2 adsorption isotherms at 77 K were recorded for activated as-synthesized **HKUST-1**, LP, and **HKUST-1@LP** xerogel (Fig. 2). **HKUST-1** exhibited a characteristic type-I isotherm indicative of microporosity, with a BET surface area of 835 m^2 g^{-1}, consistent with previously reported values.[58] LP showed a characteristic type-IVb isotherm that plateaus at high relative pressures, along with an H_2 hysteresis loop, which reveals the presence of mesopores in LP with a BET surface area of 353 m^2 g^{-1}, which matches well with the literature-reported

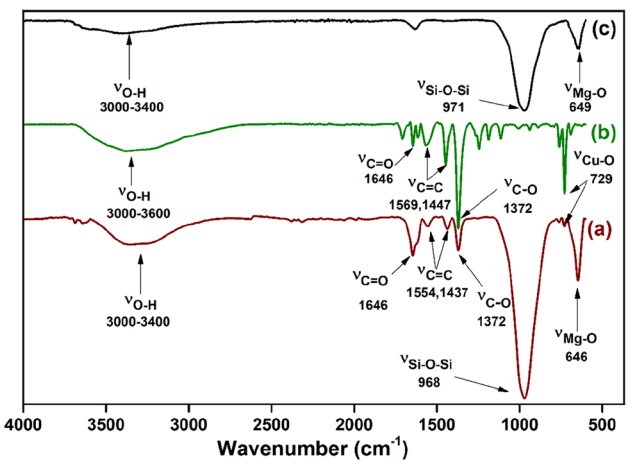

Fig. 1 FTIR spectra of (a) **HKUST-1@LP** xerogel, (b) as-synthesized **HKUST-1** and (c) LP.

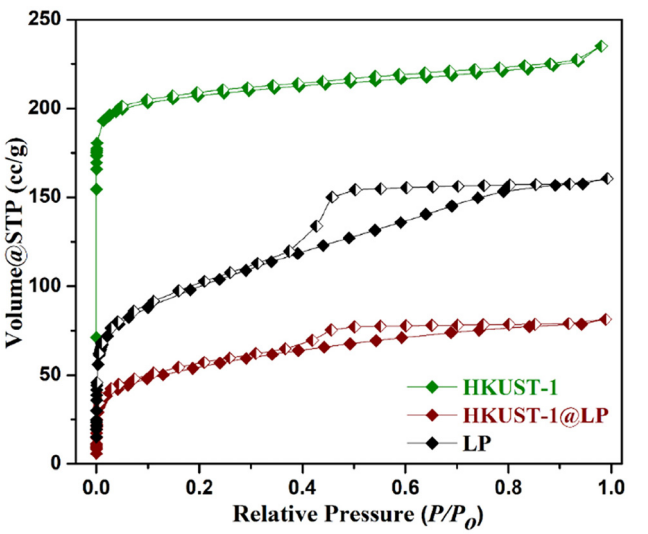

Fig. 2 N_2 adsorption isotherms of as-synthesized **HKUST-1**, **HKUST-1@LP** xerogel and LP at 77 K. Adsorption of gas molecules is denoted by open symbols while closed symbols denote desorption of gas molecules.

value.[64] The desolvated **HKUST-1@LP** xerogel exhibited a profile indicative of both microporosity and mesoporosity, owing to the presence of both **HKUST-1** and LP. The calculated BET surface area of the composite xerogel was found to be 194 $m^2\ g^{-1}$. The reduction in surface area compared to both the parent materials is attributed to the fact that the MOF particles are embedded/wrapped within layers of LP (Fig. S5), similar to the literature-reported ZIF-8–LP composite.[33] Such wrapping may lead to the partial blockage or reduced accessibility of the intrinsic pores of **HKUST-1**. As a result, although **HKUST-1** itself possesses a large surface area, its porous network is not fully available for gas adsorption once incorporated into the composite matrix, which diminishes the overall porosity of the composite.

Zeta potential measurements

Zeta potential measurements were carried out to understand the stability and surface charge properties of pure LP and **HKUST-1**. The zeta potentials were found to be −31.61 mV and −12.56 mV for LP and **HKUST-1**, respectively, at neutral pH (*i.e.* 7), and the values match well with those found in the literature.[33,57]

The zeta potential value of **HKUST-1@LP** xerogel is −19 mV at pH = 7, which shows a less negative value compared to that of pure LP but is more negative than that of **HKUST-1**. This further supports our conjecture that the negatively charged surface of **HKUST-1** and the positively charged facets of LP undergo charge-assisted self-assembly to form the composite gel.

Rheology study

Rheology data of LP and the **HKUST-1@LP** hydrogel were recorded to provide insight into the gel's stability and mechanical strength. This typically involved measuring viscoelastic properties, such as variations in storage modulus (G') and loss modulus (G'') with respect to both frequency and strain (Fig. 3). Frequency sweep measurements revealed parallel and linear G' and G'' curves for LP and the **HKUST-1@LP** hydrogel (Fig. 3a). In addition, G' and G'' of hydrogels were also examined against applied strain (%) at a constant frequency (1 Hz) for both LP and **HKUST-1@LP** (Fig. 3b). The decrease in G' with increasing stress indicates partial breakdown of the hydrogels, with notable structural failure occurring at yield stress levels of 52.7% and 82.7% for LP and **HKUST-1@LP** hydrogel, respectively. This underscores that the **HKUST-1@LP** hydrogel shows enhanced mechanical robustness compared to that of LP.[46,49]

Dye adsorption studies

MOFs have emerged as incredibly promising adsorbent materials for the capture and removal of dyes because of their exceptionally large surface area, tunable porosity, and chemical diversity. MOF-based dye adsorption and separation is a very successful wastewater treatment and environmental protection technique, reducing chemical waste and facilitating dye recovery for industrial reuse.[43]

In our work, we measured adsorption capacities of three adsorbents, *i.e.*, LP, as-synthesized **HKUST-1**, and

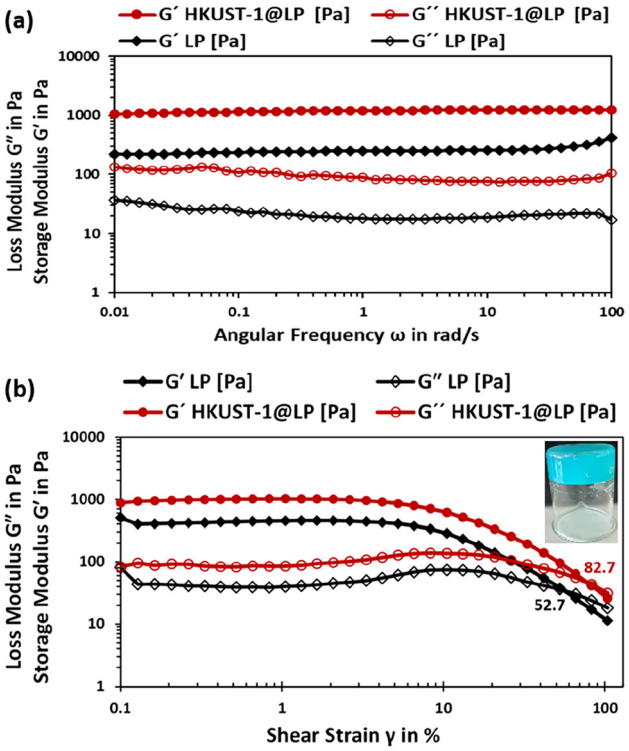

Fig. 3 (a) At a constant strain of 1%, the frequency sweep rheological experiment for LP and **HKUST-1@LP** hydrogel in MeOH/H_2O and (b) at a constant frequency of 1 Hz, the strain amplitude rheological experiment for LP and **HKUST-1@LP** hydrogel in MeOH/H_2O. Inset: image of the inverted beaker representing stable gel formation.

HKUST-1@LP xerogel using three dyes, including two cationic dyes (MB and RhB), and one anionic dye, methyl orange (MO). The study involves a detailed analysis of the adsorption behavior through saturation plots, focusing on the differences between cationic (MB and RhB) and anionic (MO) dyes (Fig. 4 and S8–S10). The colour of the solution gradually changes during the adsorption process (stirred at 25 °C) for the respective dye, indicating a progressive decrease in dye concentration over time (0 to 1500 minutes). This trend suggests an interaction between the adsorbate dyes and the adsorbent sample, facilitating dye adsorption. The detailed analysis of the plots revealed that dye adsorption increases with an increase in time for each sample adsorbent and it can be concluded that among the different adsorbents, the **HKUST-1@LP** xerogel exhibits maximum adsorption capacity for all the dyes, compared to that of LP and **HKUST-1**. The adsorption capacity values at different times (q_t mg g^{-1}) for all the samples were determined (Fig. 5 and Table 1). The **HKUST-1@LP** xerogel shows adsorption of MB, RhB, and MO with maximum adsorption capacity values for each dye of 229 mg g^{-1}, 212 mg g^{-1}, and 23 mg g^{-1} corresponding to absorbance maxima at 664 nm, 553 nm, and 464 nm, respectively, up to 1500 minutes. On the other hand, LP exhibits a maximum adsorption of 108 mg g^{-1} and 97 mg g^{-1} for MB and RhB, respectively (Table 1). A negligible adsorption was obtained for

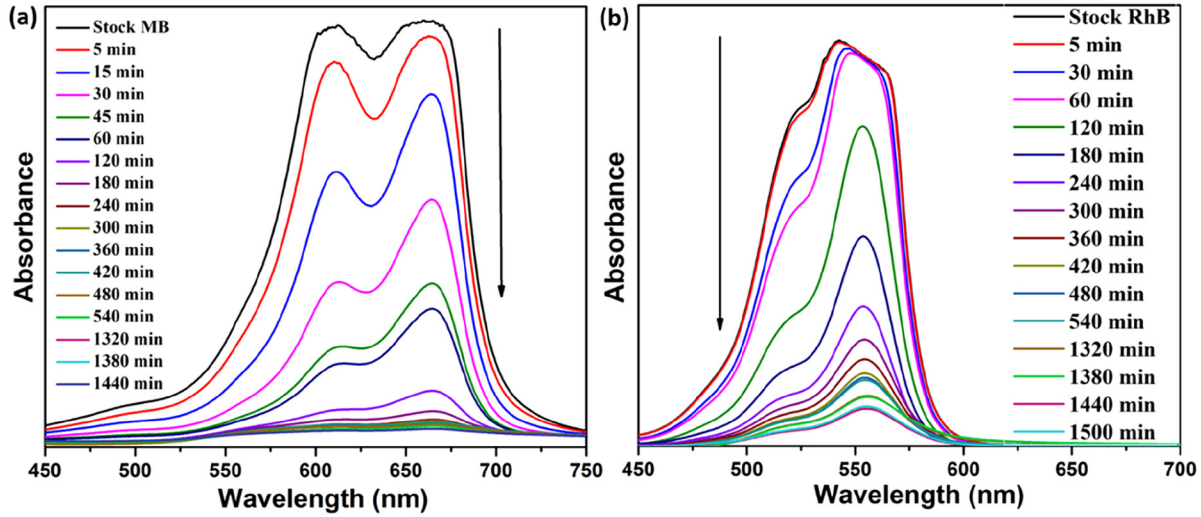

Fig. 4 UV-vis plots of dye adsorption using **HKUST-1@LP** xerogel: (a) MB and (b) RhB dyes.

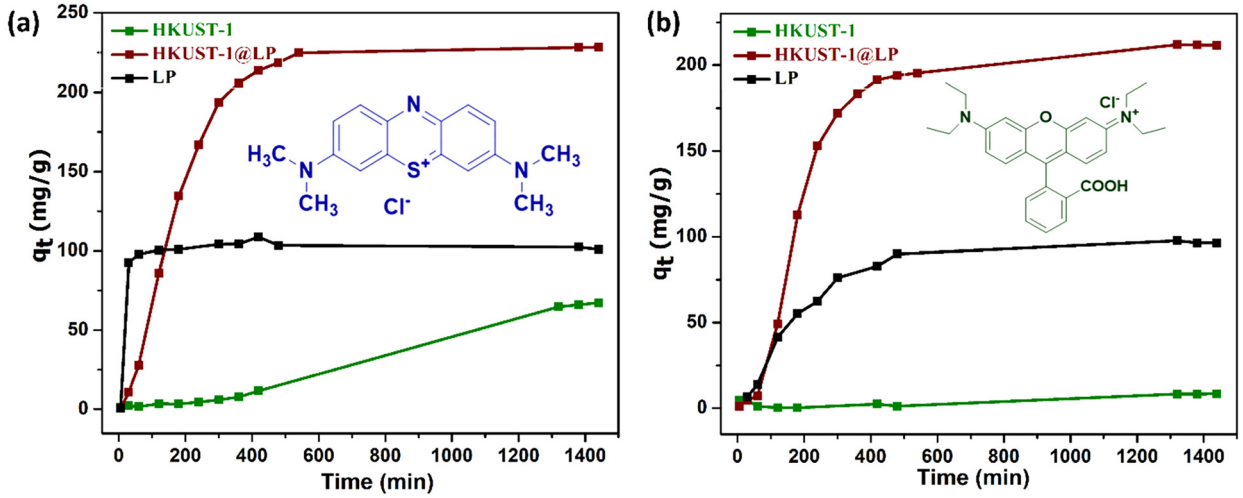

Fig. 5 Loading curves of (a) MB and (b) RhB using **HKUST-1**, LP and **HKUST-1@LP** xerogel.

Table 1 Amount of dye adsorbed (mg g^{-1}) by different adsorbents[a]

Serial no.	Adsorbates	Adsorbents	Dye adsorbed (mg g^{-1})
1	MB	**HKUST-1@LP**	**229**
2	RhB	**HKUST-1@LP**	212
3	MO	**HKUST-1@LP**	23
4	MB	LP	108
5	RhB	LP	97
6	MO	LP	1
7	MB	**HKUST-1**	67
8	RhB	**HKUST-1**	8
9	MO	**HKUST-1**	Negligible

[a] Reaction conditions: 15 mg adsorbent, 100 ml (35 ppm) aqueous dye solution, stirred at 25 °C for up to 1500 minutes.

the negatively charged dye MO, owing to the repulsion between the dye and LP particles having negatively charged facets. After maximum adsorption of the dye, saturation was reached in 1440–1500 minutes, suggesting the equilibrium condition was reached during this time span. Once equilibrium is reached, we may conclude that all available adsorptive sites in the framework have become saturated and no further dye adsorption occurs. **HKUST-1** shows adsorption of MB and RhB dyes with adsorption capacities 67 mg g^{-1} and 8 mg g^{-1}, respectively, and negligible adsorption was observed for MO (Table 1 and Fig. S10). Under equilibrium conditions, the removal efficacy of MB for **HKUST-1@LP** xerogel was found to be superior among all three adsorbents (Table 1). The results for **HKUST-1@LP** xerogel further demonstrate that MB undergoes the highest adsorption, followed by RhB, while MO

exhibits minimal adsorption. This is attributed to the strong electrostatic interaction between the cationic dye and the nucleophilic environment of the composite, as indicated by its negative zeta potential (−19 mV). This explains the higher adsorption capacity for MB, therefore enabling its efficient adsorption. The rapid adsorption of MB might also be supported by its smaller size and linear structure. In contrast, RhB, although a cationic dye, shows less adsorption than MB because of its larger size and non-linear structure. The electrostatic repulsion between the negatively charged gel network and the anionic dye molecules predominantly prevents the adsorption of MO, therefore causing minimal uptake.

For effective wastewater treatment, it is not only essential for the adsorbent to exhibit high adsorption capacity for individual dye pollutants, but also to efficiently remove a selected dye from their mixtures, and separation efficacy remains a significant challenge. Beyond single-dye adsorption studies, we also investigated the adsorption behavior of the composite using dye mixtures to assess its selectivity (Fig. 6 and Fig. S11). **HKUST-1@LP** xerogel was soaked in a mixture of MB/MO, MB/RhB, and MO/RhB dye solutions and time-dependent UV-vis studies indicated that molecules of MB were adsorbed more efficiently than those of MO or RhB dyes over a set range of times.

Table S3 presents the dye adsorption capacities of literature-reported MOFs and MOF-based composites and compares the data with the dye adsorption performance of **HKUST-1@LP** xerogel and also suggests that dye adsorption efficacy of **HKUST-1@LP** xerogel is found to be noteworthy compared to the pristine MOFs and other MOF-based composites. We envisage that the **HKUST-1@LP** composite, owing to its gel-like network structure and the synergistic contributions of the parent materials, exhibits enhanced dye adsorption capacity and superior separation efficiency. For the effective adsorptive removal of wastewater contaminants, the availability of adsorptive sites of the adsorbent plays an essential role. However, other key factors also influence the adsorption capacity, including the surface area of the adsorbent sample, the linearity of dye molecules, the charge and size of the dye molecules, and the surface charge of the framework.[65–68] Typically, the adsorption–desorption phenomenon is driven by electrostatic interactions between the adsorbate and adsorbent, π–π interactions, hydrogen bonding, non-covalent interactions, van der Waals forces, and ion exchange processes.[66] For the **HKUST-1@LP** xerogel, the adsorption mechanism may predominantly involve electrostatic interactions, hydrogen bonding, and π–π interactions.[34,53–55] The high adsorption capacity for MB can be attributed to the strong electrostatic attraction between the cationic MB^+ molecules and the nucleophilic aromatic moieties of carboxylate groups present in the MOF framework. H-bonding interactions between O^- (present in both the LP and MOF) and protons of the dyes and π–π interactions between the aromatic ring of dye molecules and the MOF also contribute significantly to the overall adsorption process. Similar to MB, the cationic RhB dye is significantly adsorbed by the composite, since both interact through the same types of interactions such as π–π, electrostatic, and H-bonding. The interactions between the composite and the dye molecules are illustrated in Scheme 2.

Gel-column chromatographic separation of organic dyes

Inspired by the selectivity in dye capture of the composite, we further investigated its efficacy to serve as a stationary phase for gel-column chromatographic separation of dyes. It may be noted that several studies have reported the use of MOFs as stationary phases in column chromatography for separating various compounds, including organic molecules, dyes and other pollutants.[69–80] However, the use of MOF-based hydrogels as a stationary phase in gel-column chromatography for dye separation remains unexplored. Keeping in mind the unique combination of high and selective dye adsorption, water retention properties and processability of the hydrogel composite **HKUST-1@LP**, we envisaged that it could be a

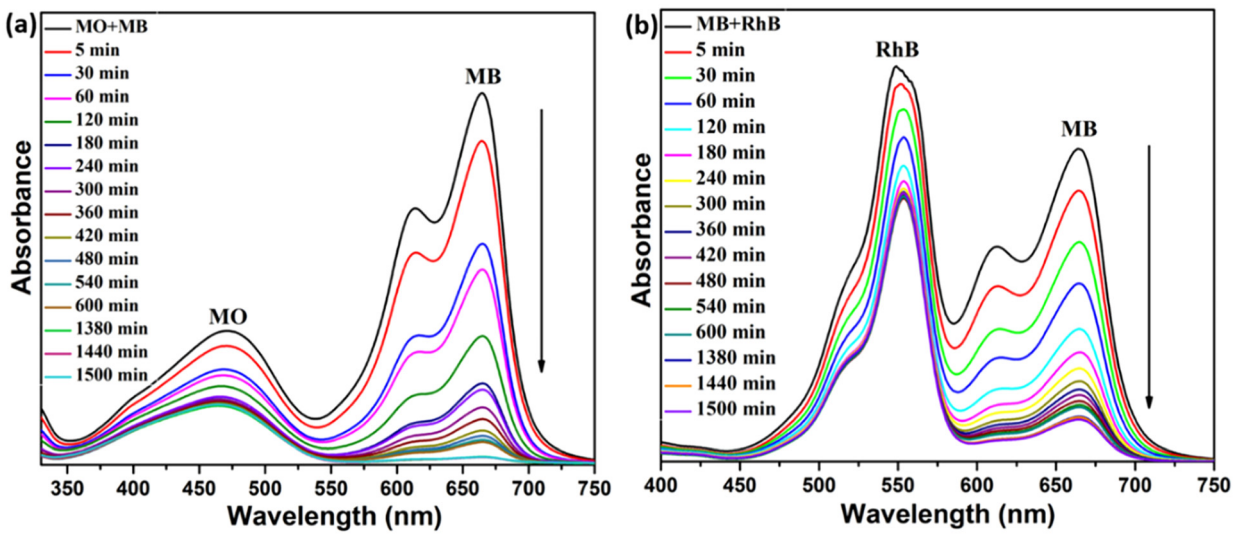

Fig. 6 UV-vis plots of selective dye adsorption from a mixture of (a) MO/MB and (b) MB/RhB dyes by **HKUST-1@LP** xerogel.

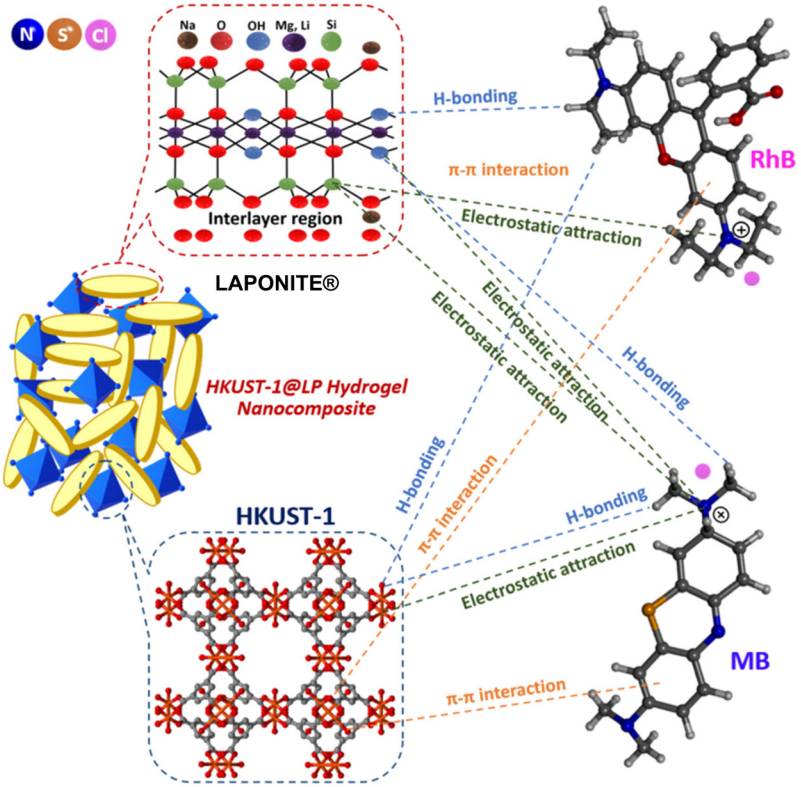

Scheme 2 Schematic illustration showing the plausible interactions between the **HKUST-1@LP** xerogel and the dye molecules.

promising material for improving dye separation efficiency in wastewater treatment in a selective manner. MO, an anionic dye, and MB, a cationic dye, were chosen for their distinct visual properties. Initial adsorption studies revealed that the hydrogel could fully adsorb the cationic dye MB from a 10^{-5} M solution but not the anionic dye MO, as confirmed by UV-vis spectrophotometry. To demonstrate chromatographic separation, a column (15 cm length and 0.5 cm bore diameter) was packed with the **HKUST-1@LP** hydrogel for use as the stationary phase, and a mixture of MO and MB in methanol was passed through it. Owing to electrostatic repulsion where the xerogel composite has a negative zeta potential, the anionic MO dye was eluted steadily, turning the column yellow initially. Once the MO dye had fully eluted in 450 minutes, the column turned blue, indicating the adsorption of MB by the hydrogel (Fig. 7). This selective adsorption of MB can be attributed to the electrostatic interaction between the positively charged dye and the negatively charged surface of the

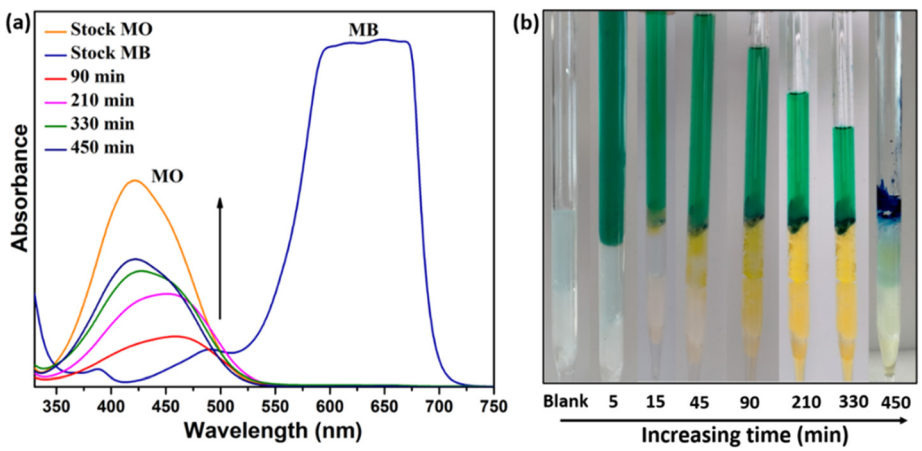

Fig. 7 (a) Comparison of absorption spectra of eluent indicating gradual separation of MO from MB dye and (b) colour of the column changes with time indicating separation of MO and MB dye from their mixture using the nanocomposite **HKUST-1@LP**.

HKUST-1@LP hydrogel, showcasing the hydrogel's effectiveness in separating cationic dyes from mixtures based on charge interactions. UV-vis spectra of eluted dye with time were recorded until all of the dye was separated from the mixture (Fig. 7). Additionally, the composite hydrogel's ability to differentiate between cationic dyes was further evaluated using a mixture of MB and RhB dyes in methanol (Fig. S12). The results show that while MB was fully adsorbed by the **HKUST-1@LP** hydrogel, RhB was only partially eluted. This partial elution of RhB suggests that separation efficiency is influenced not only by charge interactions but also by other factors such as molecular size and specific affinity to the MOF structure. This finding highlights the hydrogel's potential to selectively separate dyes within complex mixtures, providing insight into tailoring composite materials for targeted pollutant removal. Furthermore, to evaluate the separation efficiency of the **HKUST-1@LP** hydrogel relative to silica as a stationary phase, column chromatographic separation was performed using the same dye mixture (MO/MB). When silica was used, dyes eluted rapidly within minutes, hindering effective separation. This rapid elution highlights the limited retention capability of silica, whereas the **HKUST-1@LP** hydrogel demonstrates superior dye selectivity and controlled separation.

The facile formation of thin films could be a remarkable advantage of such sol–gel phases. Next, we attempted the formation of a **HKUST-1@LP** hydrogel film by a spin-coating method.

HKUST-1@LP hydrogel can be facilely spin-coated onto a glass substrate at 4000 rpm for 2 minutes. The coated film slide was air-dried and then AFM was conducted to check the topographical properties of the film. The film exhibits very good uniformity at the overall surface (Fig. S13a) and the 3D view of the surface is displayed in Fig. S13b. The AFM measurements were performed in contact mode using a SiO_2

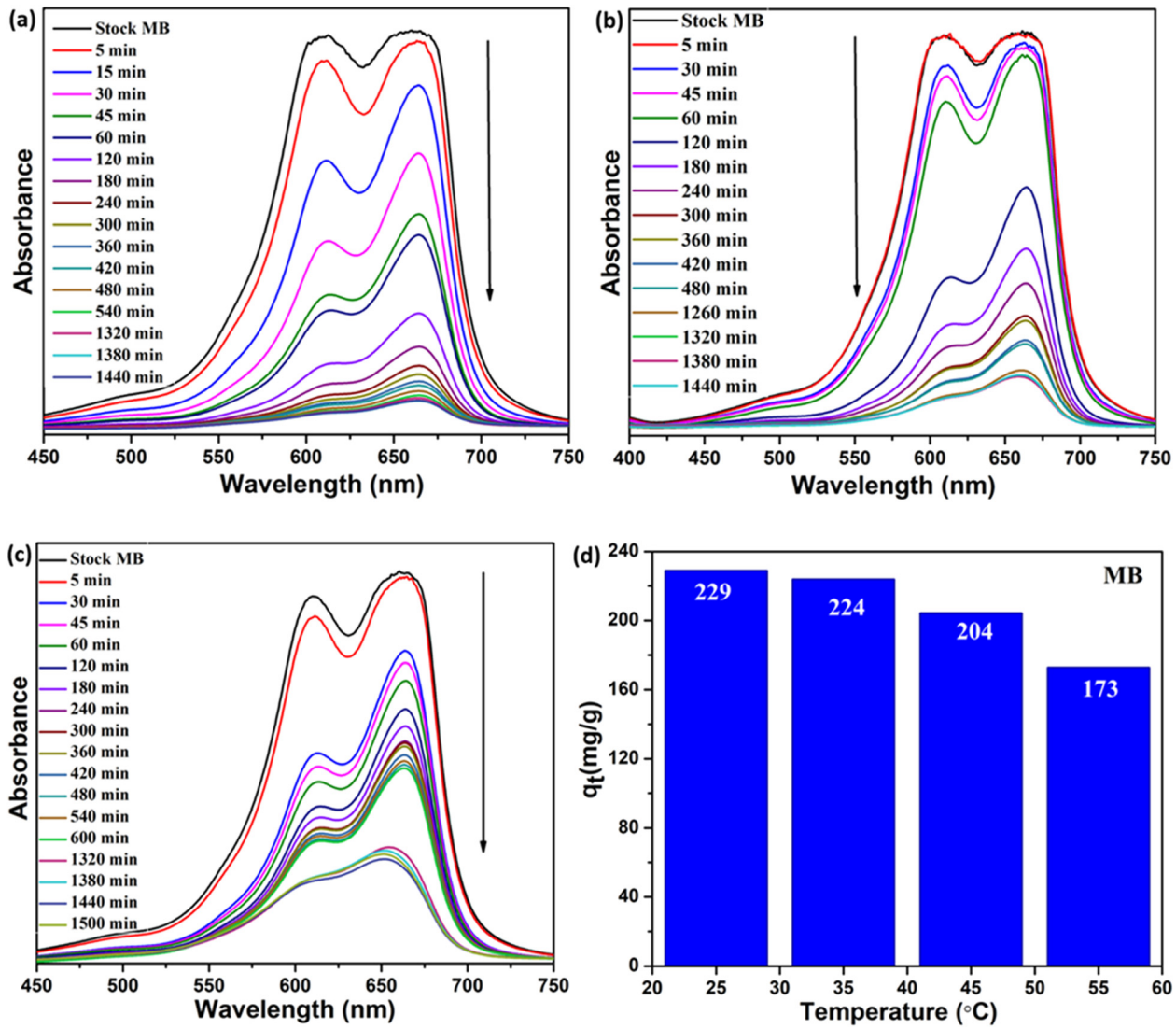

Fig. 8 UV-vis plots of MB dye adsorption using **HKUST-1@LP** xerogel at (a) 35 °C, (b) 45 °C, (c) 55 °C and (d) bar diagram showing the amount of dye adsorbed (MB) at different temperatures.

tip with a force constant value of 0.2 N m^{-1}. The surface roughness calculated using Tosca analysis software was 23.7 nm, which confirms the good uniformity of the film formation.

Effect of temperature and adsorption kinetics

Temperature is a crucial physicochemical parameter that influences the adsorption capacity of dye molecules. We conducted a detailed study of the adsorption–desorption phenomena at varying temperatures. Generally, as the temperature increases, the adsorption capacity tends to decrease, indicating that the process is exothermic.[53] The highest adsorption capacity of **HKUST-1@LP** xerogel for MB dye motivated us to examine the adsorption capacities for MB at different temperatures within the range of 25 °C to 55 °C. As presented in Fig. 8, the adsorption efficiency of the **HKUST-1@LP** xerogel for MB dye diminishes with rising temperatures from 25 °C to 55 °C. This may be attributed to increased molecular motion at higher temperatures, which creates sufficient hindrance to reduce the adsorption of dye molecules within the MOF framework.[53] It was found that 25 °C is the optimum temperature at which maximum adsorption is observed.

The adsorption behavior of MB using the **HKUST-1@LP** composite is influenced by the contact time between the adsorbent and the dye molecules. To evaluate this process, the pseudo-second-order kinetics model was employed[81] (for details see the SI). It should be noted that we tested different models, such as pseudo-first-order and pseudo-second-order equations, and it was the pseudo-second-order equation that exhibited the highest correlation coefficient (R^2), indicating the best fit for the experimental data. This suggests that the adsorption mechanism is primarily governed by chemisorption rather than physical diffusion. The linearity of the kinetic plot (Fig. S14) further reinforces the applicability of the pseudo-second-order model in describing the adsorption dynamics of MB using **HKUST-1@LP**. A linear plot of $\ln k_2$ *versus* $1/T$ for MB adsorption using **HKUST-1@LP** xerogel was constructed to determine the activation energy (E_a) from the slope (Fig. S15). The activation energy was also calculated by thermodynamic parameters with the help of k_2 calculated at different temperatures using the Arrhenius equation[82] and was found to be 59.49 kJ mol^{-1} (see the SI).

Conclusion

In summary, a new MOF–clay composite hydrogel (**HKUST-1@LP**), was synthesized *via* the self-assembly of **HKUST-1** and LP and the composite provides an efficient and selective separation approach through gel-column chromatography. We envisaged that the electrostatic interactions between the negatively charged surface of **HKUST-1** and the positively charged facets of LP facilitate the formation of the composite. The resultant material demonstrates superior adsorption capabilities, particularly for cationic dyes such as MB and RhB, as well as great dye separation performance, as evidenced by gel-column chromatography. Additionally, the composite hydrogel showcases enhanced mechanical robustness, with significantly elevated storage and loss moduli compared to values for the pristine LP, and the ability to withstand greater strain before structural failure enhances the performance of the composite. Our findings underscore the potential of emerging MOF–clay chemistry to furnish functional hydrogel composites by facile synthetic routes. Such composites may demonstrate great promise for advanced applications in dye adsorption and separation processes, offering versatile solutions for environmental and industrial challenges.

Experimental

Materials

All commercially available chemicals were used without further purification. Copper nitrate trihydrate ($Cu(NO_3)_2{\cdot}3H_2O$) and trimesic acid (H_3BTC) were purchased from Sigma-Aldrich Chemical Company. LAPONITE® (LP) was gratefully provided by BYK India Private Limited. Distilled water, acetone, ethanol, methanol, methyl orange (MO), methylene blue (MB) and rhodamine B (RhB) were purchased from Central Drug House (CDH), Delhi.

Physical measurements

PXRD patterns were recorded using a Rigaku Smart Lab SE instrument with Cu-Kα radiation (λ = 1.5406 Å). FTIR spectra were recorded on a Bruker IFS 66v/S spectrophotometer within the 4000–500 cm^{-1} range. Thermal stability under an N_2 atmosphere was assessed using a Mettler Toledo-TGA 850 instrument, with measurements conducted from 30 to 800 °C at a heating rate of 5 °C min^{-1}. Morphological studies were performed using a Zeiss GeminiSEM 500 Field Emission Electron Microscope, with samples placed on a silicon wafer under high vacuum and subjected to an accelerating voltage of 20 kV. Elemental composition was analyzed *via* EDS using an EDAX Genesis instrument attached to the FESEM column. Adsorption isotherms of N_2 at 77 K were measured using an AUTOSORB iQ2 instrument with desolvated samples. To prepare these samples, LP, **HKUST-1**, and **HKUST-1@LP** xerogel were degassed at 120 °C under a 10^{-1} Pa vacuum for 12 hours prior to measurement. To examine dye adsorption, UV-vis spectroscopy was employed. The instrument used was a Shimadzu UV-2600 spectrophotometer equipped with quartz cells. Surface height topography was observed *via* atomic force microscopy (AFM) using an Anton Paar AFM. A silicon probe with resonant frequency of 14 kHz and a force constant of 0.2 N m^{-1} was used for nanomechanical characterization. The zeta potential measurements for all the samples were carried out using a NanoZS (Malvern, UK) employing a 532 nm laser.

Synthetic procedure

HKUST-1. HKUST-1 was synthesized following a literature-reported procedure.[58] In brief, $Cu(NO_3)_2{\cdot}3H_2O$ (378 mg, 1.8 mmol) was dissolved in 18 ml of water, and 18 ml aqueous suspension of trimesic acid (H_3BTC) (210 mg, 0.9 mmol) was quickly added to this solution. The reaction mixture was then

vigorously stirred at 1200 rpm for 1 hour at 25 °C. The resulting product was collected, washed three times with ethanol, and then subjected to sonication and centrifugation at 9000 rpm for 12 minutes. The sample was subsequently dried under vacuum. The yield was 42% relative to Cu(II) salt. The phase purity of the sample was verified using PXRD (Fig. S1).

Gelation experiments and stability of the HKUST-1 phase in the composite gel

HKUST-1@LP hydrogel. This study explores the gelation behavior of **HKUST-1** and LP at room temperature by varying their ratios (Table S1). The hydrogel nanocomposite formulation involved an *ex situ* synthetic process, starting with preparing a stock solution of **HKUST-1**, *i.e.*, 20 mg of **HKUST-1** was dispersed in 4 ml of methanol by sonication for about 45 minutes at 35 °C. Simultaneously, 16 mg of LP was dispersed in 1 ml of water. Following this, 500 μl of the **HKUST-1** suspension was added to the LP solution under sonication at 35 °C, resulting in the rapid formation of a stable hydrogel, termed **HKUST-1@LP** (Table S1, entry 2). To prepare a larger batch of the composite, the stock solution of **HKUST-1** (20 mg in 4 ml of MeOH) was introduced into the LP dispersion, which contained 128 mg of LP in 8 ml of water, during sonication. The sonication process continued for approximately 15 minutes at 35 °C, after which the mixture was left undisturbed. Over the course of 3–5 days, stable hydrogel formation occurred. The hydrogel remained structurally intact upon inversion (Fig. S2), indicating strong and stable gel network formation. All the characterization studies were carried out using **HKUST-1@LP** xerogel except the rheology studies.

Stability of the HKUST-1 phase in the composite gel

To understand the chemical stability of the **HKUST-1** phase in the composite, we carried out additional experiments and treated the as-synthesized **HKUST-1** sample under conditions identical to those of the composite synthesis. Specifically, 20 mg of **HKUST-1** was dispersed in 4 ml of methanol by sonication for about 45 minutes at 35 °C. This stock solution of **HKUST-1** (20 mg in 4 ml of MeOH) was immersed in 8 ml of water and sonicated. The resulting mixture was allowed to stand for 2 minutes, and an identical batch was prepared and left to stand for 1 hour. Afterward, the samples were centrifuged, and the MOF solids were collected and dried. The dried materials were analyzed by PXRD. The obtained diffraction patterns (Fig. S3b) clearly show that the characteristic diffraction peaks of **HKUST-1** are retained, confirming that the **HKUST-1** framework does not undergo decomposition under the applied conditions. These results verify the chemical integrity and structural stability of **HKUST-1** within the composite.

Dye adsorption

Batch adsorption experiments. Three dyes MB, MO, and RhB were used to assess the adsorption capacity of all samples. 15 mg of each adsorbent (LP, **HKUST-1** and **HKUST-1@LP** xerogel) were immersed individually in 100 ml of freshly prepared aqueous dye solutions with an initial concentration of 35 ppm. Furthermore, to evaluate dye adsorption selectivity, mixed-dye solutions (MB/MO, MB/RhB, and MO/RhB) were prepared separately by dissolving 3.5 mg of each dye in 100 ml of water (35 ppm). Subsequently, 15 mg of **HKUST-1@LP** xerogel was added to 100 ml of each mixed-dye solution. Over a set time range of 0–1500 minutes, UV-vis spectroscopy was used to track the adsorption behavior of the samples. Magnetic stirring ensured the solutions were constantly stirred during the experiments; aliquots were extracted at predetermined time intervals. With UV-vis spectra recorded in the 185–800 nm range, each sample aliquot was examined individually. Eqn (1) was used to compute the adsorbed dye amount, q_e (mg g^{-1}):[81]

$$q_e = \frac{(C_0 - C_e)V}{m} \quad (1)$$

Here, C_0 (mg L^{-1}) and C_e (mg L^{-1}) represent the initial and equilibrium concentrations of the dye in solution, respectively. V (L) denotes the volume of the dye solution, while m (mg) corresponds to the mass of the adsorbent used. The effect of temperature on the adsorption behavior of all samples, as well as the removal rate of MB, MO, and RhB dyes from aqueous solutions, was investigated using UV-vis spectrophotometry.

Conflicts of interest

There are no conflicts to declare.

Data availability

The data supporting this article have been included as part of the supplementary information (SI). Supplementary information: PXRD patterns, TGA plots, FESEM images, particle size histogram, elemental mapping, UV-vis spectra, chromatography column images, AFM images, kinetics plots and tables. See DOI: https://doi.org/10.1039/d5dt02005k.

Acknowledgements

A. C. sincerely acknowledges the Department of Science and Technology (DST), New Delhi, India, for an INSPIRE Faculty Fellowship (DST/INSPIRE/04/2020/001603). Jyoti acknowledges UGC, New Delhi, for a Senior Research Fellowship (NTA ref. no.: 221610140712). Chhaya acknowledges CSIR, New Delhi, for a Junior Research Fellowship (file no.: 09/1152(21555)/2025-EMR-I). The authors gratefully acknowledge Prof. Tapas Kumar Maji and Mr Soumya Kanti Mondal of JNCASR, Bangalore, for conducting some of the measurements.

References

1 H.-C. Zhou, J. R. Long and O. M. Yaghi, *Chem. Rev.*, 2012, **112**, 673, DOI: 10.1021/cr300014x.

2 P. Falcaro, R. Ricco, C. M. Doherty, K. Liang, A. J. Hill and M. J. Styles, *Chem. Soc. Rev.*, 2014, **43**, 5513, DOI: 10.1039/C4CS00089G.
3 V. Stavila, A. A. Talin and M. D. Allendorf, *Chem. Soc. Rev.*, 2014, **43**, 5994, DOI: 10.1039/C4CS00096J.
4 C. Ashworth, *Nat. Rev. Mater.*, 2017, **2**, 17074, DOI: 10.1038/natrevmats.2017.74.
5 P. Kanoo, R. Haldar, P. Sutar, A. Chakraborty and T. K. Maji, *Functional Supramolecular Materials: From Surfaces to MOFs*, The Royal Society of Chemistry, 2017, ch. 12, p. 412. DOI: 10.1039/9781788010276-00412.
6 T. Islamoglu, Z. Chen, M. C. Wasson, C. T. Buru, K. O. Kirlikovali, U. Afrin, M. R. Mian and O. K. Farha, *Chem. Rev.*, 2020, **120**, 8130, https://pubs.acs.org/doi/10.1021/acs.chemrev.9b00828.
7 S. Roy, A. Chakraborty and T. K. Maji, *Coord. Chem. Rev.*, 2014, **273**, 139, DOI: 10.1016/j.ccr.2014.03.035.
8 P. Yadav, P. Bhardwaj, M. Maruthi, A. Chakraborty and P. Kanoo, *Dalton Trans.*, 2023, **52**, 11725, DOI: 10.1039/D3DT01301D.
9 P. Yadav, S. Kumari, A. Yadav, P. Bhardwaj, M. Maruthi, A. Chakraborty and P. Kanoo, *ACS Omega*, 2023, **8**, 28367, https://pubs.acs.org/doi/10.1021/acsomega.3c02418.
10 A. Yadav, S. Kumari, P. Yadav, A. Hazra, A. Chakraborty and P. Kanoo, *Dalton Trans.*, 2022, **51**, 15496, DOI: 10.1039/D2DT02098J.
11 A. Yadav and P. Kanoo, *Chem. – Asian J.*, 2019, **14**, 3531, DOI: 10.1002/asia.201900876.
12 P. Cheng, C. Wang, Y. V. Kaneti, M. Eguchi, J. Lin, Y. Yamauchi and J. Na, *Langmuir*, 2020, **36**, 4231, DOI: 10.1021/acs.langmuir.0c00236.
13 W. Zhang, X. Wu, X. Peng, Y. Tian and H. Yuan, *Adv. Mater.*, 2025, **37**, 2412708, DOI: 10.1002/adma.202412708.
14 J. Hou, A. F. Sapnik and T. D. Bennett, *Chem. Sci.*, 2020, **11**, 310, DOI: 10.1039/c9sc04961d.
15 L. Zhu, L. Zong, X. Wu, M. Li, H. Wang, J. You and C. Li, *ACS Nano*, 2018, **12**, 4462, DOI: 10.1021/acsnano.8b00566.
16 S. Furukawa, J. Reboul, S. Diring, K. Sumida and S. Kitagawa, *Chem. Soc. Rev.*, 2014, **43**, 5700, DOI: 10.1039/c4cs00106k.
17 T. Tian, J. Velazquez-Garcia, T. D. Bennett and D. Fairen-Jimenez, *J. Mater. Chem. A*, 2015, **3**, 2999, DOI: 10.1039/C4TA05116E.
18 Jyoti, S. Kumari, S. Chakraborty, P. Kanoo, V. Kumar and A. Chakraborty, *Dalton Trans.*, 2024, **53**, 15815, DOI: 10.1039/D4DT00849A.
19 A. Chakraborty, Jyoti and T. K. Maji, *Dalton Trans.*, 2025, **54**, 433, DOI: 10.1039/D4DT02789B.
20 A. Chakraborty, S. Laha, K. Kamali, C. Narayana, M. Eswaramoorthy and T. K. Maji, *Inorg. Chem.*, 2017, **56**, 9426, https://pubs.acs.org/doi/10.1021/acs.inorgchem.7b01601.
21 A. Chakraborty, S. Roy, M. Eswaramoorthy and T. K. Maji, *J. Mater. Chem. A*, 2017, **5**, 8423, DOI: 10.1039/C6TA09886J.
22 A. Chakraborty, A. Achari, M. Eswaramoorthy and T. K. Maji, *Chem. Commun.*, 2016, **52**, 11378, DOI: 10.1039/C6CC05289D.
23 J. Y. C. Lim, L. Goh, K. Otake, S. S. Goh, X. J. Loh and S. Kitagawa, *Biomater. Sci.*, 2023, **11**, 2661, DOI: 10.1039/d2bm01906j.
24 X. Huang, Q. Qin, Q. Ma and B. Wang, *Water*, 2022, **14**, 3487, DOI: 10.3390/w14213487.
25 X. Hou, J. Sun, M. Lian, Y. Peng, D. Jiang, M. Xu, B. Li and Q. Xu, *Macromol. Mater. Eng.*, 2023, **308**, 2200469, DOI: 10.1002/mame.202200469.
26 J. Zhang, X. He, Y.-R. Kong, H.-B. Luo, M. Liu, Y. Liu and X.-M. Ren, *ACS Appl. Mater. Interfaces*, 2021, **13**, 37231, DOI: 10.1021/acsami.1c11054.
27 S. Li and F. Huo, *Nanoscale*, 2015, **7**, 7482, DOI: 10.1039/C5NR00518C.
28 Q.-L. Zhu and Q. Xu, *Chem. Soc. Rev.*, 2014, **43**, 5468, DOI: 10.1039/c3cs60472a.
29 P. Cheng, C. Wang, Y. V. Kaneti, M. Eguchi, J. Lin, Y. Yamauchi and J. Na, *Langmuir*, 2020, **36**, 4231, DOI: 10.1021/acs.langmuir.0c00236.
30 P. Sutar and T. K. Maji, *Inorg. Chem.*, 2017, **56**, 9417, https://pubs.acs.org/doi/10.1021/acs.inorgchem.7b01002.
31 P. Sutar and T. K. Maji, *Chem. Commun.*, 2016, **52**, 13136, DOI: 10.1039/C6CC06971A.
32 P. Sutar, V. M. Suresh, K. Jayaramulu, A. Hazra and T. K. Maji, *Nat. Commun.*, 2018, **9**, 3587, DOI: 10.1038/s41467-018-05818-w.
33 A. Chakraborty, P. Sutar, P. Yadav, M. Eswaramoorthy and T. K. Maji, *Inorg. Chem.*, 2018, **57**, 14480, DOI: 10.1021/acs.inorgchem.8b02545.
34 K. Maru, S. Kalla and R. Jangir, *New J. Chem.*, 2022, **46**, 3054, DOI: 10.1039/d1nj05015j.
35 L. Wang, H. Xu, J. Gao, J. Yao and Q. Zhang, *Coord. Chem. Rev.*, 2019, **398**, 213016, DOI: 10.1016/j.ccr.2019.213016.
36 L. Heinke, M. Tu, S. Wannapaiboon, R. A. Fischer and C. Wöll, *Microporous Mesoporous Mater.*, 2015, **216**, 200, DOI: 10.1016/j.micromeso.2015.03.018.
37 J. Liu and C. Wöll, *Chem. Soc. Rev.*, 2017, **46**, 5730, DOI: 10.1039/c7cs00315c.
38 D. Zacher, R. Schmid, C. Wöll and R. A. Fischer, *Angew. Chem., Int. Ed.*, 2011, **50**, 176, DOI: 10.1002/anie.201002451.
39 S. Schmitt, S. Diring, P. G. Weidler, S. Begum, S. Heißler, S. Kitagawa, C. Wöll, S. Furukawa and M. Tsotsalas, *Chem. Mater.*, 2017, **29**, 5982, DOI: 10.1021/acs.chemmater.7b01677.
40 J. J. Marrero-Tellado and D. D. Díaz, *CrystEngComm*, 2015, **17**, 7978, DOI: 10.1039/c5ce01032b.
41 T. Guo, H. Mashhadimoslem, L. Choopani, M. M. Salehi, A. Maleki, A. Elkamel, A. Yu, Q. Zhang, J. Song, Y. Jin and O. J. Rojas, *Small*, 2024, **20**, 2402942, DOI: 10.1002/smll.202402942.
42 Y. Li, G. Wen, J. Li, Q. Li, H. Zhang, B. Tao and J. Zhang, *Chem. Commun.*, 2022, **58**, 11488, DOI: 10.1039/D2CC04190A.
43 S. Sağlam, F. N. Türk and H. Arslanoğlu, *J. Environ. Chem. Eng.*, 2023, **11**, 110568, DOI: 10.1016/j.jece.2023.110568.
44 S. Jatav and Y. M. Joshi, *Appl. Clay Sci.*, 2014, **97–98**, 72, DOI: 10.1016/j.clay.2014.06.004.

45 Q. Wang, J. L. Mynar, M. Yoshida, E. Lee, M. Lee, K. Okuro, K. Kinbara and T. Aida, *Nature*, 2010, **463**, 339, DOI: 10.1038/nature08693.
46 U. Šebenik, R. Lapasin and M. Krajnc, *Carbohydr. Polym.*, 2020, **240**, 116330, DOI: 10.1016/j.carbpol.2020.116330.
47 D. W. Thompson and J. T. Butterworth, *J. Colloid Interface Sci.*, 1992, **151**, 236, DOI: 10.1016/0021-9797(92)90254-J.
48 S. S. Das, Neelam, K. Hussain, S. Singh, A. Hussain, A. Faruk and M. Tebyetekerwa, *Curr. Pharm. Des.*, 2019, **25**, 424, DOI: 10.2174/1381612825666190402165845.
49 H. A. Baghdadi, J. Parrella and S. R. Bhatia, *Rheol. Acta*, 2008, **47**, 349, DOI: 10.1007/s00397-007-0236-1.
50 J. Labanda and J. Llorens, *Colloids Surf., A*, 2004, **249**, 127, DOI: 10.1016/j.colsurfa.2004.08.063.
51 H. Tomás, C. S. Alves and J. Rodrigues, *Nanomedicine*, 2018, **14**, 2407, DOI: 10.1016/j.nano.2017.04.016.
52 P. Sutar, V. R. Bakuru, P. Yadav, S. Laha, S. B. Kalidindi and T. K. Maji, *Chem. – Eur. J.*, 2021, **27**, 3268, DOI: 10.1002/chem.202004345.
53 I. Mantasha, H. A. M. Saleh, K. M. A. Qasem, M. Shahid, M. Mehtab and M. Ahmad, *Inorg. Chim. Acta*, 2020, **511**, 119787, DOI: 10.1016/j.ica.2020.119787.
54 S. Lin, Z. Song, G. Che, A. Ren, P. Li, C. Liu and J. Zhang, *Microporous Mesoporous Mater.*, 2014, **193**, 27, DOI: 10.1016/j.micromeso.2014.03.004.
55 M. Ş. A. Eren, H. Arslanoğlu and H. Çiftçi, *J. Environ. Chem. Eng.*, 2020, **8**, 104247, DOI: 10.1016/j.jece.2020.104247.
56 Y. Li, C. Gao, J. Jiao, J. Cui, Z. Li and Q. Song, *ACS Omega*, 2021, **6**, 33961, DOI: 10.1021/acsomega.1c0529947.
57 L. Zhao, X. Duan, M. R. Azhar, H. Sun, X. Fang and S. Wang, *Chem. Eng. J. Adv.*, 2020, **1**, 100009, DOI: 10.1016/j.ceja.2020.100009.
58 J. Huo, M. Brightwell, S. E. Hankari, A. Garai and D. Bradshaw, *J. Mater. Chem. A*, 2013, **1**, 15220, DOI: 10.1039/C3TA14409G.
59 Z.-Q. Xiong, X.-D. Li, F. Fu and Y.-N. Li, *Pet. Sci.*, 2019, **16**, 890, DOI: 10.1007/s12182-018-0298-y.
60 J. Zhang, C. Su, X. Xie, P. Liu and Md. E. Huq, *RSC Adv.*, 2020, **10**, 37028, DOI: 10.1039/D0RA05275b.
61 C. Xin, H. Zhan, X. Huang, H. Li, N. Zhao, F. Xiao, W. Wei and Y. Sun, *RSC Adv.*, 2015, **5**, 27901, DOI: 10.1039/c5ra03986j.
62 Z. Liu, Z. Zhao, X. Jin, L.-M. Wang and Y. D. Liu, *Molecules*, 2021, **26**, 1482, DOI: 10.3390/molecules26051482.
63 Negrete, J.-M. Letoffe, J.-L. Putaux, L. David and E. Bourgeat-Lami, *Langmuir*, 2004, **20**, 1564, DOI: 10.1021/la0349267.
64 H. Pálková, J. Madejová, M. Zimowska, E. Bielańska, Z. Olejniczak, L. Lityńska-Dobrzyńska and E. M. Serwicka, *Microporous Mesoporous Mater.*, 2010, **127**, 228, DOI: 10.1016/j.micromeso.2009.07.019.
65 S. Song, C. Hao, X. Zhang, Q. Zhang and R. Sun, *Open Chem.*, 2018, **16**, 1283, DOI: 10.151s5/chem-2018-0137.
66 J. Shen, X. Wang, L. Zhang, Z. Yang, W. Yang, Z. Tian, J. Chen and T. Tao, *J. Cleaner Prod.*, 2018, **184**, 949, DOI: 10.1016/j.jclepro.2018.03.015.
67 M. Danish, T. Ahmad, R. Hashim, N. Said, M. N. Akhtar, J. Mohamad-Saleh and O. Sulaiman, *Surf. Interfaces*, 2018, **11**, 1, DOI: 10.1016/j.surfin.2018.02.001.
68 X. Fan, W. Wang, W. Li, J. Zhou, B. Wang, J. Zheng and X. Li, *ACS Appl. Mater. Interfaces*, 2014, **6**, 14994, https://pubs.acs.org/doi/10.1021/am5028346.
69 T. Si, X. Lu, H. Zhang, S. Wang, X. Liang and Y. Guo, *TrAC, Trends Anal. Chem.*, 2022, **149**, 116545, DOI: 10.1016/j.trac.2022.116545.
70 B. Kharisov, O. Kharissova, V. Zhinzhilo, J. Bryantseva and I. Uflyand, *Appl. Sci.*, 2022, **12**, 12219, DOI: 10.3390/app122312219.
71 C.-X. Yang, S.-S. Liu, H.-F. Wang, S.-W. Wang and X.-P. Yan, *Analyst*, 2012, **137**, 133, DOI: 10.1039/c1an15600d.
72 S.-R. Zhang, J. Li, D.-Y. Du, J.-S. Qin, S.-L. Li, W.-W. He, Z.-M. Su and Y.-Q. Lan, *J. Mater. Chem. A*, 2015, **3**, 23426, DOI: 10.1039/C5TA07427D.
73 C. Yao, W. Wang, S.-R. Zhang, H.-Y. Li, Y.-H. Xu, Z.-M. Su and G.-B. Che, *RSC Adv.*, 2018, **8**, 36400, DOI: 10.1039/c8ra04648d.
74 R. Ameloot, A. Liekens, L. Alaerts, M. Maes, A. Galarneau, B. Coq, G. Desmet, B. F. Sels, J. F. M. Denayer and D. E. De Vos, *Eur. J. Inorg. Chem.*, 2010, **2010**, 3735, DOI: 10.1002/ejic.201000494.
75 M. Liu, Y. Jing, L. Zhang, Y. Zhou, H. Yan, Y. Song and X. Qiao, *J. Chromatogr. B*, 2021, **1163**, 122506, DOI: 10.1016/j.jchromb.2020.122506.
76 K. Yusuf, A. Aqel and Z. ALOthman, *J. Chromatogr. A*, 2014, **1348**, 1, DOI: 10.1016/j.chroma.2014.04.095.
77 R. Kaur, A. Kaur, A. Umar, W. A. Anderson and S. K. Kansal, *Mater. Res. Bull.*, 2019, **109**, 124, DOI: 10.1016/j.materresbull.2018.07.025.
78 Y. Yu, Y. Ren, W. Shen, H. Deng and Z. Gao, *TrAC, Trends Anal. Chem.*, 2013, **50**, 33, DOI: 10.1016/j.trac.2013.04.014.
79 S.-N. Zhao, C. Krishnaraj, H. S. Jena, D. Poelman and P. V. D. Voort, *Dyes Pigm.*, 2018, **156**, 332, DOI: 10.1016/j.dyepig.2018.04.023.
80 A. Ahmed, M. Forster, R. Clowes, D. Bradshaw, P. Myers and H. Zhang, *J. Mater. Chem. A*, 2013, **1**, 3276, DOI: 10.1039/c2ta01125e.
81 W.-P. Wu, J. Wu, J.-Q. Liu, M. Trivedi and A. Kumar, *RSC Adv.*, 2017, **7**, 54522, DOI: 10.1039/c7ra11221a.
82 M. Alkan, Ö. Demirbaş and M. Doğan, *Microporous Mesoporous Mater.*, 2007, **101**, 388, DOI: 10.1016/j.micromeso.2006.12.007.